

Attosecond metrology

M. Hentschel*†, R. Kienberger*†, Ch. Spielmann*, G. A. Reider*, N. Milosevic*, T. Brabec*, P. Corkum‡, U. Heinzmann§, M. Drescher§ & F. Krausz*

* Institut für Photonik, Technische Universität Wien, Gusshausstr. 27, A-1040 Wien, Austria

‡ Steacie Institute of Molecular Sciences, NRC Canada, Ottawa, Canada K1A 0R6

§ Fakultät für Physik, Universität Bielefeld, D-33615 Bielefeld, Germany

† These authors contributed equally to this work

The generation of ultrashort pulses is a key to exploring the dynamic behaviour of matter on ever-shorter timescales. Recent developments have pushed the duration of laser pulses close to its natural limit—the wave cycle, which lasts somewhat longer than one femtosecond (1 fs = 10⁻¹⁵ s) in the visible spectral range. Time-resolved measurements with these pulses are able to trace dynamics of molecular structure, but fail to capture electronic processes occurring on an attosecond (1 as = 10⁻¹⁸ s) timescale. Here we trace electronic dynamics with a time resolution of ≤ 150 as by using a subfemtosecond soft-X-ray pulse and a few-cycle visible light pulse. Our measurement indicates an attosecond response of the atomic system, a soft-X-ray pulse duration of 650 ± 150 as and an attosecond synchronism of the soft-X-ray pulse with the light field. The demonstrated experimental tools and techniques open the door to attosecond spectroscopy of bound electrons.

Experimental access to fast-evolving microscopic processes requires a short excitation ('pump') pulse, which sets the process going, and a short probe pulse for taking snapshots of the evolution of the process¹. Recent advances in ultrafast optics have made available laser pulses as short as a few femtoseconds for this time-resolved (or pump–probe) measurement technique^{2,3}. These pulse durations are practically at the limit set by the laser field oscillation cycle in the visible spectral range. They allow the tracking of changes in the nuclear structure of molecules—such as vibrations, or the breaking and formation of chemical bonds—because the characteristic timescale for atomic motion on an atomic length scale (0.1 nm) extends from a few femtoseconds to a few thousand femtoseconds (refs 4, 5). But time-domain access to a wide range of electron dynamics in the atomic shells has been frustrated so far by the speed of electronic relaxation processes. The wavefunction of bound electrons, following an energetic excitation—for example, ionization or the creation of an inner-shell vacancy—tends to evolve on an attosecond timescale. Until now, insight into these processes could be gained only indirectly from frequency-domain measurements of transition linewidths⁶.

Coherent extreme-ultraviolet (XUV) and X-ray sources are not only important tools for atomic spectroscopy but, owing to their short wave cycle, also offer the potential for producing electromagnetic radiation of attosecond duration. High-order harmonics of femtosecond laser radiation^{7,8} have been recently shown to be^{9,10} sources of trains of attosecond XUV pulses, separated by one half-cycle of the laser period with the train extending over some 10 fs. Yet, attosecond time-resolved measurements still appeared to be out of reach, because straightforward interpretation of spectroscopic data requires isolated, single pulses^{11,12}. Moreover, the XUV fluences available from current high-harmonic sources are many orders of magnitude lower than required by XUV-pump/XUV-probe spectroscopy, while conventional schemes of visible-light/XUV cross-correlation, yielding a convolution of the respective pulse envelopes, do not provide subfemtosecond time resolution. Using few-cycle visible laser pulses¹³ for the generation of isolated soft-X-ray pulses¹⁴, together with a special geometry for detecting photoelectrons originating from atoms exposed simultaneously to both of these pulses, our work offers a way to overcome these limitations.

Here we report the observation of light-field-induced petahertz frequency (1 PHz = 10¹⁵ Hz) modulation of the width of the kinetic energy distribution of photoelectrons; these photoelectrons were derived from an atomic gas (krypton, in our experiments) excited

by an ultrashort 90-eV soft-X-ray (henceforth briefly X-ray) pulse. Our measurements yield an X-ray pulse duration of $\tau_x = 650 \pm 150$ as, and indicate that more than 90% of the X-ray photons, which are spectrally filtered by a bandpass at ~ 90 eV, are confined within a single, isolated pulse of this duration. The experimental results bear direct evidence of the X-ray pulse being synchronized to the field oscillations of the visible light pulse with attosecond precision; they also indicate bound–free electronic transitions from the $4p$ state of krypton responding to 90-eV excitation on an attosecond timescale. With these tools we have traced the electric field oscillations in a visible light wave with a resolution of better than 150 as. These measurements constitute, to our knowledge, the first demonstrations of attosecond metrology. Beyond measuring the duration of X-ray pulses with attosecond resolution, our approach will permit attosecond spectroscopy of bound electron dynamics in atoms and molecules using a low-fluence subfemtosecond X-ray pulse and a strong visible light field.

X-ray photoemission controlled by a strong light field

Angle-resolved X-ray-induced photoemission assisted by visible light has been recently used to measure the cross-correlation of the intensity envelope of a 7-fs visible light pulse with that of an ultrashort soft-X-ray pulse¹⁴. Drawing on this previous work, we show here control of the final kinetic energy of X-ray-generated photoelectrons by the oscillating light field rather than by its cycle-averaged intensity. This enables us to probe, on an attosecond timescale, the duration of the X-ray pulse and its timing jitter with respect to the light field. The key to this progress has been (1) an approach that allows us to combine an enhanced solid angle of detection with attosecond temporal resolution, and (2) matching the X-ray pulse front to the light wave front within the volume of their interaction with nanometre-scale precision and stability. Photoelectrons from atoms exposed simultaneously to a strong light field and an X-ray pulse were detected within a cone aligned orthogonally to the beam direction and electric field vector of the linearly polarized light field. This orthogonal detection geometry was chosen to suppress a background in the photoelectron spectrum produced primarily along the electric field vector of the light pulse by above-threshold ionization (ATI).

The effect of the light field on the X-ray photoelectron energy spectrum is now well understood in a quantum-mechanical framework^{15,16}. In the strong-field limit, the most conspicuous features can also be accounted for by a quasi-classical model treating the interaction as a two-step process¹⁴: first, the photoelectron is

ejected by a short X-ray pulse with a distribution of initial momenta known from conventional photoionization studies⁶; and second, the photoelectron is subsequently accelerated as a classical particle by the electric field of a femtosecond light pulse. In accordance with the quantum treatment, the model predicts that, depending on the oscillation phase of the light field at the instant of ‘birth’ of the electron, a momentum component along the electric field vector, Δp_x , is added to the initial momentum of the electron, resulting in a shift of the photoelectron distribution up or down in momentum space (Fig. 1). The momentum transfer gives rise to a spread of the final kinetic energy of photoelectrons collected within a finite solid angle as revealed by the top and bottom of Fig. 1. The effect increases with increasing detection cone and vanishes for monodirectional detection.

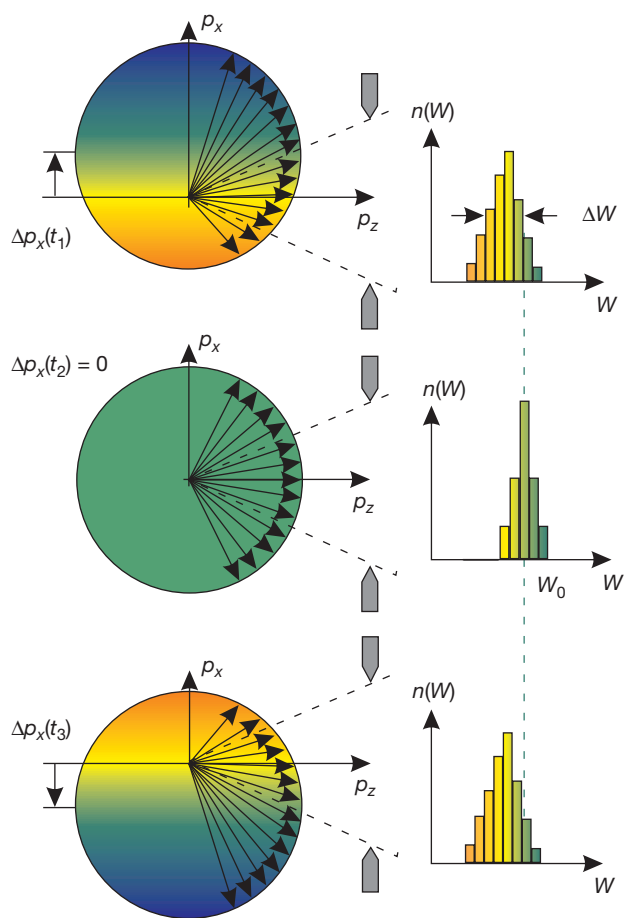


Figure 1 The principle of measuring cross-correlation between light electric field and X-ray intensity with attosecond resolution by means of ‘two-colour’ photoionization. The photoelectrons created initially with isotropic momentum distribution by the absorption of X-ray photons pick up momentum from the strong femtosecond laser field. In the slowly varying wave approximation, the field-induced momentum change Δp_x depends on the phase, amplitude and oscillation frequency of the light electric field at the instant of birth and is independent of the subsequent evolution of the light field. At birth instants t_1 , $t_2 = t_1 + T_0/4$ and $t_3 = t_1 + T_0/2$ chosen such that the light field crosses zero at t_1 and t_3 , the light-induced momentum change Δp_x deforms the final photoelectron momentum and energy distribution as shown. Different colours represent electrons of different final kinetic energy, with the energy increasing from the red to the blue. The momentum transfer and hence the change in the energy spectrum is largest if the electric field of the light pulse crosses zero at the moment of birth of the photoelectron (top and bottom). For a birth instant coinciding with the peak of the light electric field (centre) the final energy spectrum is unaffected by the light field and is determined by the spectrum of the X-ray pulse (represented by a single colour and a well-defined radius of the sphere in momentum space for simplicity).

Scanning the instant of birth of the photoelectron through the light field oscillations by changing the relative delay t_d between the light pulse and X-ray pulse results in a modulation of the spectral width $\Delta W(t_d)$ with a period equal to one-half of the light oscillation period T_0 . Figure 1 reveals that a confined detection cone aligned orthogonally to the light field vector also gives rise to a downshift of the centre of gravity of the photoelectron spectrum. This energy shift was used in our earlier study as a primary observable¹⁴. The key advantage of exploiting instead the broadening of the spectrum is that this effect is enhanced by increasing the detection aperture, and thus allows for a significantly enhanced signal yield and modulation amplitude. By contrast, the modulation in the centre of gravity of the photoelectron spectrum gets increasingly washed out with increasing detection angle, resulting in deterioration of the temporal resolution.

In the above description, we tacitly assumed an X-ray pulse duration τ_x that was very short compared to $T_0/2$, as well as an instantaneous response of the electronic transition, defining precisely the instant of birth of the photoelectron on a timescale of $T_0/2$. A finite X-ray pulse duration and timing jitter of the X-ray pulse (relative to the phase of the light field) of any origin results in a reduced depth of the above-discussed modulation of $\Delta W(t_d)$. In fact, an X-ray pulse duration approaching $T_0/2$ smears out the modulation completely. Our results rely on this line of argument: the modulation depth of $\Delta W(t_d)$ sets a reliable upper limit, on an attosecond timescale, on the X-ray pulse duration and timing jitter.

Cross-correlation of light electric field and X-ray intensity

The experiments reported below have been performed with a modified version of the apparatus described previously¹⁴. Major modifications included an enhanced detection angle and the installation of a feedback-controlled piezo delay stage as well as X-ray beam diagnostics. Figure 2 illustrates schematically the main steps in creating and processing the X-ray and light pulses for the photoemission experiment discussed in the preceding section.

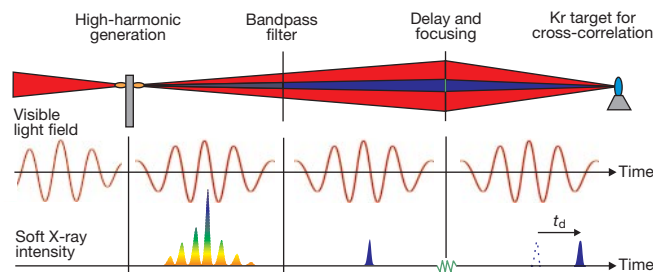


Figure 2 Diagram of the principal physical effects and processes preceding our light-field-controlled X-ray photoemission experiment. First, the few-cycle visible light pulse interacts with a jet of neon atoms to produce a train of pulses in the XUV and soft-X-ray spectral range. The rainbow colours of the individual pulses symbolize the respective spectral energy content: the highest photon energy components are contained only in a single pulse generated near the peak of the driver pulse. Note the increase of the instantaneous frequency in the centre of the visible light pulse (addressed as a dynamic blue shift in the text) past the interaction due to self phase modulation in the laser-generated plasma. The collinear laser and soft-X-ray beams are passed through a small circular Zr filter matched in size to the diameter of the harmonic beam. It stops the central portion of the laser beam, and transmits the low-divergence harmonic beam near 90 eV along with an annular laser beam surrounding it. The two co-axial beams then are focused onto the Kr atomic gas target by a concentric piezo-controlled double mirror unit¹⁴ (rays actually reflected at this point are unfolded in our schematic illustration for convenience). The central Mo/Si reflector serves simultaneously as a focusing mirror for the 90-eV soft-X-ray harmonics, and as a bandpass filter that selects the highest-energy photons contained only in the central harmonic pulse. Furthermore, this multifunctional unit provides the necessary adjustable delay between the visible light and soft-X-ray harmonic pulse.

The kinetic energy spectrum of 4*p* photoelectrons ejected from krypton atoms under simultaneous irradiation by the 90-eV X-ray pulse ($\lambda \approx 14$ nm) and the light pulse ($\lambda \approx 750$ nm) driving the harmonic radiation was measured as a function of t_d , which is the delay between the X-ray and the light pulse, both polarized along the x direction in Fig. 1. The Kr 4*p* electrons were chosen because of their favourable yield along the z direction at our X-ray photon energies⁶. The light pulse (peak intensity, $\sim 5 \times 10^{13}$ W cm⁻²) overlapped with the more tightly focused X-ray pulse in a volume of krypton gas kept at a pressure of a few times 10⁻² mbar, limited to this value to prevent space-charge effects. The detection cone of our time-of-flight spectrometer is defined by the aperture of the spectrometer and its distance from the krypton target, with its full angle limited to $\sim 40^\circ$ by the numerical aperture of the electron lens system employed.

The delay was varied in steps of $\Delta t_d = 150$ as in the central range of temporal overlap (-5 fs $\leq t_d \leq 5$ fs, with $t_d = 0$ near the peak of the light pulse), and in larger steps outside this range. Figure 3 shows two representative Kr 4*p* spectra corrected for an ATI background and recorded at $t_d = -450$ as and $t_d = 0$, along with respective asymmetric gaussian fits. This model function yields excellent fits to our data, characterized by a fidelity parameter $R^2 > 0.95$. The noise increasing to lower energies can be attributed to ATI electrons. The contour plot in Fig. 4 depicts a series of Kr 4*p* photoelectron spectra (processed as described above) as a function of delay t_d . The data clearly bring to light a quasi-periodic evolution of the photoelectron energy spectrum. Both the width and, as a consequence of normalization to constant area, the peak height of the photoelectron energy spectrum are subject to a modulation versus t_d at a period of $\sim T_0/2$. Coupled to a modulation of the spectral width, we observe a periodic downshift of the centre of gravity of the spectrum, in agreement with our model's (Fig. 1) prediction for a narrow detection solid angle. However, the spectral shift is found to be contaminated by much larger uncertainties than is the variation of the spectral width.

For a quantitative analysis, we study the width of the photoelectron spectrum ΔW as a function of t_d . The upper panel of Fig. 4 shows the variation of the full-width at half-maximum $\Delta W(t_d)$ of the gaussian fits versus delay between the X-ray and light pulse. In what follows we focus on the oscillatory part of $\Delta W(t_d)$, which was obtained by subtracting the cycle-averaged 'd.c.' component of $\Delta W(t_d)$. The result is depicted by dots in Fig. 5 along with the respective error bars. From an inspection of the error bars at points of maximum slope in Fig. 5, we infer a time resolution of our

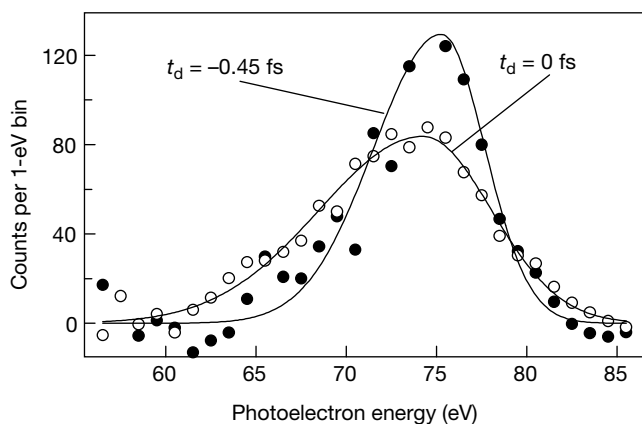


Figure 3 Kr 4*p* photoelectron spectra produced by ~ 90 -eV soft-X-ray pulses in the presence of a strong visible light field at two different delays t_d of the X-ray pulse. (Positive t_d corresponds to a retardation of the X-ray pulse.) The dots represent results corrected for ATI background. The lines show asymmetric gaussian fits to the data. The spectra were acquired over a measurement time of 2 minutes each.

sampling scheme of ≤ 150 as. The modulation period of the data is close to 1.25 fs in the wings of the correlation function $\Delta W(t_d)$, in agreement with a carrier wavelength of ~ 750 nm of the light pulse. However, it decreases to ~ 0.9 fs near zero delay, indicative of a pronounced blue shift of the light pulse at its peak, the origin of which we shall discuss below.

Subfemtosecond X-ray pulse

To evaluate the X-ray pulse duration from our light-field/X-ray-intensity cross-correlation data (dots in Fig. 5), we simulated the light-field-induced variation of the Kr 4*p* photoelectron spectrum versus t_d based on the quasi-classical model described above. The duration τ_x of our gaussian model X-ray pulse was used as the only fit parameter. In the analytic representation of the light pulse, the pronounced frequency upshift at the pulse centre and a small residual chirp apparent in the measured correlation function $\Delta W(t_d)$ was taken into account as described in the caption of Fig. 5. Under the assumption of an isotropic initial momentum distribution of X-ray photoelectrons and a uniform detection efficiency within the aperture of the spectrometer, our simple model reproduces well all observed key features (oscillating broadening and downshift of the photoelectron spectrum) except for a pronounced asymmetry of the broadened spectra.

The red line in Fig. 5 shows the results of our model calculations for an X-ray pulse length of $\tau_x = 650$ as, which—using no fit parameter other than τ_x —constitutes the best fit to the measured data in the range of maximum modulation depth (-1 fs $\leq t_d \leq 2$ fs). The inset displays, in addition, the computed correlation function $\Delta W(t_d)$ for $\tau_x = 500$ as and $\tau_x = 800$ as, revealing modulations respectively significantly enhanced and suppressed with respect to the measured data. These data provide a safe estimate for the duration of our 90-eV X-ray pulse within the range of $\tau_x = 650 \pm 150$ as, with the lower limit applying under the assumption of zero timing jitter of the X-ray pulse relative to the light wave.

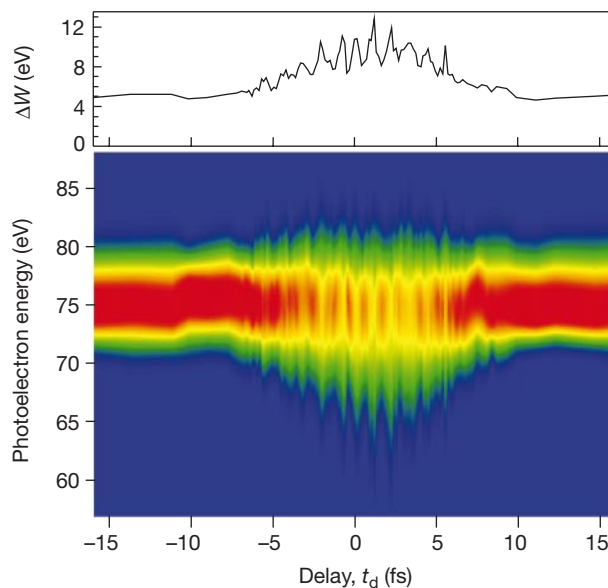


Figure 4 Cross-correlation of X-ray pulse with few-cycle laser pulse. Lower panel, contour plot of the Kr 4*p* photoelectron spectra (vertical axis) as a function of delay t_d of the soft-X-ray pulse with respect to the light pulse (horizontal axis). The plot displays the asymmetric gaussian fits introduced in Fig. 3, and comprises some 120 fitted spectra of the 4*p* feature, each normalized to the same number of counts, resulting in a constant area under the spectral distribution functions. Upper panel, spectral width ΔW evaluated from the gaussian fits as a function of the delay t_d . The spectra recorded at large delays, that is, those unaffected by the light field, are consistent with the X-ray spectrum centred at ~ 90 eV and with a binding energy of ~ 14 eV of the Kr 4*p* electron.

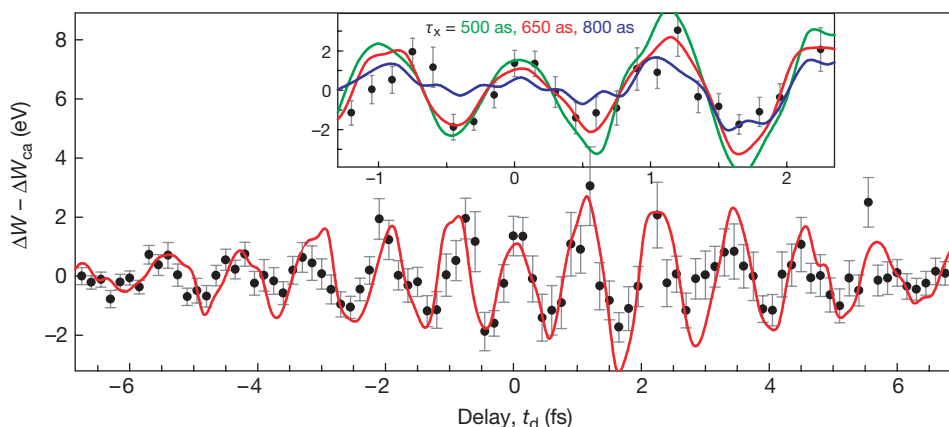


Figure 5 Spectral width ΔW of the Kr 4p photoelectron spectra as a function of t_d . The dots represent the oscillating component of the spectral width, $\Delta W - \Delta W_{ca}(t_d)$, where $\Delta W_{ca}(t_d)$ stands for the cycle-averaged value of $\Delta W(t_d)$. The full red line is the result of simulations based on the quasi-classical theory of two-colour X-ray photoionization by assuming a 7.5-fs, 750-nm linearly polarized light field of $5 \times 10^{13} \text{ W cm}^{-2}$ peak intensity and a 650-as, 90-eV gaussian X-ray pulse. The model light pulse includes a gaussian frequency sweep at the pulse peak superimposed on a weak quadratic component. Inset,

coloured lines show the result of the same simulation for different pulse durations near $t_d = 0$. The conspicuous asymmetry in the calculated and measured $\Delta W(t_d)$ about $t_d = 0$ is due to a change of the light carrier frequency occurring on a timescale T_0 . Consequently, the slowly varying wave approximation breaks down and the final state of the electron becomes dependent on the actual evolution of the light field. The substructure in the curves is an artefact, resulting from the statistical initial conditions in our simulations.

The emergence of a subfemtosecond pulse from high harmonic generation in the few-cycle regime was corroborated by numerical simulations of our X-ray source with a computer code¹⁷. This code solved Maxwell's wave equations in three dimensions and computed the radiation of the strongly-driven atomic dipoles using a generalization of the quantum treatment of ref. 18. These simulations yield a 530-as X-ray pulse near the propagation axis in the far field within a 5-eV spectral range near 90 eV (full line in Fig. 6), accompanied by a few small satellite pulses. The appearance of satellites separated by $\sim T_0/2$ from the central pulse leads to a spectral modulation with a period of twice the laser photon energy, as revealed by the calculated spectrum (full line) in the inset of Fig. 6. The depth of this modulation provides a sensitive measure of satellite content. The measured spectrum of the harmonic X-ray pulse reflected by our Mo/Si multilayer (dotted line in the inset of Fig. 6) sets a safe upper

limit of 10% to the total satellite fluence relative to the total X-ray fluence within a 5-eV range around 90 eV.

The agreement of the measured X-ray pulse duration with that obtained from our numerical calculations¹⁶ (within the experimental error) shows that the timing jitter of the X-ray pulse relative to the visible light field is much smaller than 1 fs. In other words, our experiment shows that the subfemtosecond X-ray pulse is locked to the carrier wave of its generating few-cycle light pulse with attosecond precision. This is surprising, given that the 'absolute' phase φ of the wave (defined in the caption of Fig. 6) with respect to the amplitude envelope is random in our laser pulses³, slightly modifying the evolution of the electric field from pulse to pulse. The attosecond timing stability of our subfemtosecond X-ray pulse to its few-cycle driver is due either to a (surprising) robustness of the high-harmonic generation process against these modifications, or (more likely) to a substantially reduced X-ray yield for values of φ other than the optimum assumed in Fig. 6. In the latter case, only a fraction of all laser pulses would provide an appreciable contribution to the detected photoelectron yield. If this is true, few-cycle driver pulses with stabilized absolute phase would markedly improve the data acquisition rate in the present and related experiments.

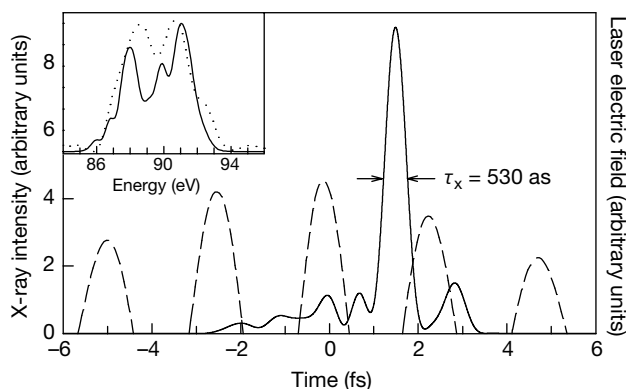


Figure 6 Calculated far-field, near-axis temporal intensity profile of a soft-X-ray pulse. The X-ray pulse is produced in a 3-mm-long 200-mbar neon gas volume by a 7-fs, 750-nm gaussian laser pulse with an on-axis peak intensity of $9 \times 10^{14} \text{ W cm}^{-2}$. For the electric field of the laser pulse, $E(t) \propto \exp(-t^2/\tau_L^2)\cos(\omega_0 t + \varphi)$ with $\varphi = 0$ (cosine pulse), where τ_L is the pulse duration, ω_0 is the angular carrier frequency and φ is the 'absolute' phase. The dashed line shows the on-axis electric field of the laser pulse leaving the interaction region. The calculated X-ray radiation is selected within a 5-eV spectral range near 90 eV. Inset, calculated (full line) and measured (dotted line) X-ray pulse spectrum selected by the Mo/Si reflector, showing that about 90% of the total fluence is within a 5-eV range around 90 eV.

Probing light-field oscillations

With its duration extracted from the central part of $\Delta W(t_d)$, the X-ray pulse can now be used, as a first application, to probe the evolution of the electric field in the light pulse. The sweep of the instantaneous carrier frequency ν_{inst} (or wavelength λ_{inst}) in the visible light pulse can be evaluated from $\Delta W(t_d)$ by fitting a sinusoidal oscillation of adjustable period to the data in Fig. 5. The dots in Fig. 7 show the carrier frequency sweep evaluated in this manner, revealing a dynamic blue shift from a carrier wavelength of $\sim 750 \text{ nm}$ to some 550 nm. To understand this phenomenon, we have to remember that the light pulse used here is derived from the one generating the X-ray pulse (Fig. 2). Also shown in Fig. 7 is the calculated frequency sweep of the laser pulse leaving the neon-gas X-ray source.

The measured dynamic frequency shift at the centre of the pulse is larger than predicted by our numerical study, but reflects qualitatively the predicted behaviour. The qualitative agreement suggests that the observed blue shift can be attributed to ionization-induced

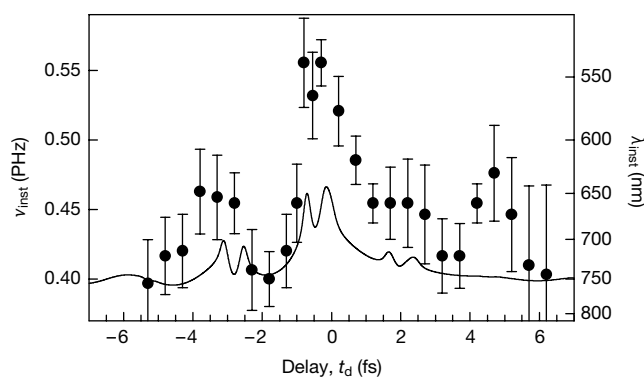


Figure 7 Calculated (line) and measured (dots) instantaneous frequency of the few-cycle light field. The experimental data are derived from $\Delta W(t_d)$ shown in Fig. 5. The computed frequency sweep originates from self-phase modulation of the light pulse upon its interaction with the neon gas X-ray source.

self-phase modulation in the X-ray generation process. These results provide evidence of optical field ionization driven by a few-cycle pulse being confined to less than one single oscillation cycle. The direct probing of the field oscillations in a light wave as implemented here is another demonstration of attosecond metrology. It should permit complete measurement of the electric field of absolute-phase-stabilized few-cycle light^{19,20}. The presence of a substantial dynamic blue shift in the light pulse used to control X-ray photoemission provides a further strong argument for the isolated nature of our X-ray pulse: the depth of modulation of $\Delta W(t_d)$ near $t_d = 0$, where the modulation period drops to ~ 0.9 fs, would rapidly decrease with increasing satellites spaced by ~ 1.25 fs from the main pulse (Fig. 6).

Attosecond spectroscopy

With the availability of single subfemtosecond X-ray pulses, it is now possible to extend time-resolved spectroscopy into the attosecond domain by using these pulses for both triggering and probing bound-bound or bound-free electronic transitions in atoms or molecules. However, the subfemtosecond X-ray pulses currently available do not yet have sufficient fluence for X-ray-pump/X-ray-probe spectroscopy. Generalization of the present concept of light-field-controlled X-ray photoemission should allow the substitution of either the X-ray pump or the X-ray probe pulse by a strong few-cycle laser field without losing attosecond resolution. This approach vastly relaxes requirements on the X-ray pulse fluence, holding promise for extending the technique up to photon energies approaching one kiloelectron volt (keV) with next-generation high-harmonic sources.

In one class of proposed experiments, an absolute-phase-stabilized¹⁹ quasi-single-cycle visible laser pulse (for example, $\tau_p = 4$ fs at $\lambda = 750$ nm, as shown by Fig. 20 in ref. 3) sets free a subfemtosecond wavepacket by optical field ionization; this wavepacket is driven back to its parent ion an optical cycle later with energies of up to a few keV and produce collisional excitations. The relaxation processes following subfemtosecond collisional excitation are important for a number of phenomena, such as X-ray lasing

and non-sequential photoionization. These processes could be traced in time by measuring the energy of photoelectrons detached from the ion by a delayed, subfemtosecond X-ray probe pulse. In another class of studies, the subfemtosecond X-ray pulse might serve as a pump pulse to create inner-shell vacancies. The temporal evolution of the subsequent inner-shell relaxation processes could be traced by time-resolved spectroscopy of the emitted Auger electron(s). The Auger spectrum, modified by a few-cycle light field and measured as a function of t_d , would provide access to the (few-femtosecond to attosecond) inner-shell relaxation times in the range of several hundred eV to keV in the same way as the correlation functions in Figs 4 and 5 yield the X-ray pulse duration. The experimental tools are now becoming available for attosecond spectroscopy. □

Received 1 October; accepted 19 October 2001.

1. Krausz, F. From femtochemistry to attophysics. *Phys. World* **14**(9), 41–46 (2001).
2. Steinmeyer, G., Sutter, D. H., Gallmann, L., Matuschek, N. & Keller, U. Frontiers in ultrashort pulse generation: pushing the limits in linear and nonlinear optics. *Science* **286**, 1507–1512 (1999).
3. Brabec, T. & Krausz, F. Intense few-cycle laser fields: frontiers of nonlinear optics. *Rev. Mod. Phys.* **72**, 545–591 (2000).
4. Zewail, A. Femtochemistry: atomic-scale dynamics of the chemical bond (adapted from the Nobel Lecture). *J. Phys. Chem. A* **104**, 5660–5694 (2000).
5. Bhattacharjee, Y. Measuring the immeasurable. *Nature* **412**, 474–476 (2001).
6. Becker, U. & Shirley, D. A. *VUV and Soft X-Ray Photoionization* 152 (Plenum, New York, 1996).
7. L’Huillier, A. & Balcou, P. High-order harmonic generation in rare gases with a 1-ps 1053-nm laser. *Phys. Rev. Lett.* **70**, 774–777 (1993).
8. Macklin, J. J., Kmetec, J. D. & Gordon, C. L. High-order harmonic generation using intense femtosecond pulses. *Phys. Rev. Lett.* **70**, 766–769 (1993).
9. Papadogiannis, N. A., Witzel, B., Kalpouzou, C. & Charalambidis, D. Observation of attosecond light localization in higher order harmonic generation. *Phys. Rev. Lett.* **83**, 4289–4292 (1999).
10. Paul, P. *et al.* Observation of a train of attosecond pulses from high harmonic generation. *Science* **292**, 1689–1692 (2001).
11. Ivanov, M., Corkum, P. B., Zuo, T. & Bandrauk, A. Routes to control of intense-field atomic polarizability. *Phys. Rev. Lett.* **74**, 2933–2936 (1995).
12. Christov, I. P., Murnane, M. M. & Kapteyn, H. C. High-harmonic generation of attosecond pulses in the “single-cycle” regime. *Phys. Rev. Lett.* **78**, 1251–1254 (1997).
13. Spielmann, Ch. *et al.* Generation of coherent X-rays in the water window using 5-femtosecond laser pulses. *Science* **278**, 661–664 (1997).
14. Drescher, M. *et al.* X-ray pulses approaching the attosecond frontier. *Science* **291**, 1923–1927 (2001). Published online 15 February 2001; 10.1126/science.1058561.
15. Kitzler, M., Milosevic, N., Scrinzi, A. & Brabec, T. Theory of attosecond streak cameras. *Phys. Rev. Lett.* (submitted).
16. Itatani, J. *et al.* Attosecond streak camera. *Phys. Rev. Lett.* (submitted).
17. Milosevic, N., Scrinzi, A. & Brabec, T. Ab initio numerical calculation of attosecond pulse generation. *Phys. Rev. Lett.* (submitted).
18. Lewenstein, M., Balcou, Ph., Ivanov, M. Yu., L’Huillier, A. & Corkum, P. B. Theory of high-harmonic generation by low-frequency laser fields. *Phys. Rev. A* **49**, 2117–2132 (1994).
19. Poppe, A. *et al.* Few-cycle optical waveform synthesis. *Appl. Phys. B* **72**, 373–376 (2001). Published online 13 December 2000; 10.1007/s003400000526.
20. Paulus, G. G. *et al.* Evidence of “absolute-phase” phenomena in photoionization with few cycle laser pulses. *Nature* **414**, 182–184 (2001).

Acknowledgements

We thank M. Uiberacker for assistance with measurements, and Y. Lim and U. Kleineberg for manufacturing the X-ray multilayer mirror. Discussions with M. Ivanov are gratefully acknowledged. This work was supported by the Austrian Science Fund and by the European ATTO network.

Competing interests statement

The authors declare that they have no competing financial interests.

Correspondence and requests for materials should be addressed to F.K. (e-mail: ferenc.krausz@tuwien.ac.at).